LA-UR-21-27538
Approved for public release; distribution is unlimited.

Title: Metal Hydride Simulations Using SWIFT

Author(s): Matthews, Christopher
Shivprasad, Aditya Prahlad
Cooper, Michael William Donald

Intended for: Report

Issued: 2021-11-08 (rev.2)

Metal Hydride Simulations Using SWIFT

Christopher Matthews, Aditya Shivprasad, and Michael Cooper

Los Alamos National Laboratory

July 2021

Contents

1 Executive Summary

Transition metal dihydrides are considered to be good candidate materials for nuclear reactor moderator applications due to their ability to maintain high hydrogen densities up to high temperatures [1]. Owing to the recent interest in metal hydrides for use in microreactor applications where the size requirements make advanced moderators exceedingly attractive, a clear need for capturing the evolving thermochemistry of these materials is evident. In an effort to provide a tool for reactor designers and experimentalists, the MOOSE-based [2] `SWIFT` code (Stoichiometry With Internally Fluctuating Temperature) has been adapted to tackle the thermochemical behavior of yttrium hydride at elevated temperatures.

While each individual piece of physics that drives the kinetics of hydrogen in metal hydrides is not in itself complex, the interconnection of the system with the gas gap and cladding results in coupled nonlinear behavior that can be nontrivial to compute. These pieces of physics, along with best estimates of material properties that are needed as input into the various mathematical descriptions of the phenomena, have been compiled here and implemented into `SWIFT`. Using only a handful of simulations, the usefulness of such a code was shown to produce plots useful for reactor designers and simulations that showed the nonlinear behavior of the non-stoichiometry within the solid YH_x.

One of the primary outcomes of this work was to show that the concentration gradient observed in metal hydrides subject to a temperature gradient cannot be attributed to a Soret type of diffusion alone; the thermochemistry of the system necessitates a complex equilibrium state across the entire material, not just at a single surface. Consequently, measurement of Soret coefficient due purely to measurement of the concentration gradient under temperature will result in a property that can accurately capture the concentration gradient as a function of the temperature gradient in only one configuration and environment, namely that of the experiment itself. As the need grows for advanced modeling and simulation to share more of the burden associated with reactor design and safety analysis, the desire for mechanistic models will continue to expand. As such, the identification of all prominent phenomena at play must be separately addressed in a realistic and meaningful manner.

2 Introduction

Transition metal dihydrides are considered to be good candidate materials for nuclear reactor moderator applications due to their ability to maintain high hydrogen densities up to high temperatures [1]. Initial work on metal hydride moderators during the Air Force Nuclear Propulsion (ANP) program enabled the development of metal hydride concepts for this application and showed that yttrium dihydride, YH_x, exhibited particularly high thermal stability, while also maintaining a relatively low neutron absorption cross-section [3]. Zirconium hydride was eventually used in the Systems for Nuclear Auxiliary Power (SNAP) program due to its much lower thermal neutron absorption cross-section, but the uranium-zirconium hydride fuel-moderator composite used in the SNAP-10A reactor slowly lost hydrogen over time due to hydrogen permeation through the moderator cladding. This slow loss resulted in a loss of 10% power over the core lifetime [4]. Another observation from studies of uranium-zirconium hydride fuel was that hydrogen redistributed from high-temperature regions to low-temperature regions, thus impacting the neutronics of the fuel-moderator composite [5]. From these initial demonstrations and studies, understanding the dynamics of hydrogen migration and loss was identified as critically important for the implementation of metal hydrides for moderator applications.

Owing to the recent interest in metal hydrides for use in microreactor applications where the size requirements make advanced moderators exceedingly attractive, a clear need for capturing the evolving thermochemistry of these materials is evident. Previous studies include numerous property measurements (see overview in [6]), with much of the modeling experience with metal hydrides established for applications as getter materials (see overview in [7]). In an effort to provide a tool for reactor designers and experimentalists, the MOOSE-based [2] `SWIFT` code (Stoichiometry With Internally Fluctuating Temperature) has been adapted to tackle the thermochemical behavior of yttrium hydride at elevated temperatures. A collection of the available data necessary for such simulations is included here, along with initial preliminary calculations that aim to provide an overview of the possible analysis that can be completed with such a tool. From these simulations, it is clear that a thermodynamically consistent nonlinear tool can help provide information to reactor designers, while also highlighting the need for further collection of quality experimental data to help refine such calculations.

3 Background

3.1 Simplified Metal Hydride Behavior

The dynamic behavior hydrogen in metal hydrides is a combination of diffusion processes and surface kinetics, regulated by the thermochemistry of the system. In order to understand the different mechanisms in play, the movement of hydrogen in metal hydrides can be broken down into several steps, here applied to yttrium dihydride YH_x, where $1.5 < x < 2$; starting with bulk YH_x, the solid material is in equilibrium with the surrounding gas when all adsorption events are balanced with an equal number of desorption events. In this way, the surface concentration of hydrogen is defined for which addition of hydrogen is equally energetically preferable in the solid as it is in the gas. This is portrayed in Fig. 3.1a for a 1-D slab of YH_x interacting via a single surface, and corresponds to the equilibrium condition for of YH_x. The equilibrium hydrogen concentration is typically established via a set of pressure, composition, and temperature curve, or PCT data. These experimentally derived curves allow the complex interplay of state variables at the surface of the metal hydride surface to determine the surface equilibrium condition.

If the temperature of the sample is increased, the corresponding equilibrium concentration of hydrogen in YH_x decreases. This is captured in Fig. 3.1b in which the surface concentration of hydrogen in the bulk material loses hydrogen in order to equilibrate with the gas. Note, Fig. 3.1b captures the instantaneous loss of hydrogen before bulk diffusion has a chance to evenly distribute the hydrogen, as in Fig. 3.1c.

Figs. 3.1a to 3.1c all represent behavior of hydrogen in an isothermal sample in communication with a reservoir of hydrogen through a single surface. If a temperature gradient is imposed across the YH_x, Soret diffusion may occur, resulting in a concentration gradient across the sample. In addition, the temperature dependence of the PCT curves will result in a spatial gradient in the surface equilibrium concentration as well, resulting in an entanglement of physics that hinders mechanistic model development.

The processes discussed in Fig. 3.1 are idealized by assuming a one-dimensional case with solid YH_x interacting with a hydrogen-containing gas through a single surface. In reality, more complex geometry complicates this simplified model. For example, Fig. 3.2a shows the full diffusion lifecycle of hydrogen starting with desorption out of YH_x, mixed into a gas plenum with a partial pressured defined by the ideal gas law, transport through a cladding that is controlled by the permeability of the cladding material, and eventual loss to the larger system which can typically be treated as a "vacuum" with respect to the hydrogen partial pressure. In addition, if more than one surface of the bulk YH_x material is free to interact with a gas environment – a situation that is nearly always the case – the thermodynamics of the system will promote a concentration gradient in the presence of a temperature gradient due to the temperature dependence of the surface equilibrium concentration.

While Fig. 3.1 is useful to understand the fundamental behavior of hydrogen in YH_x, it is the

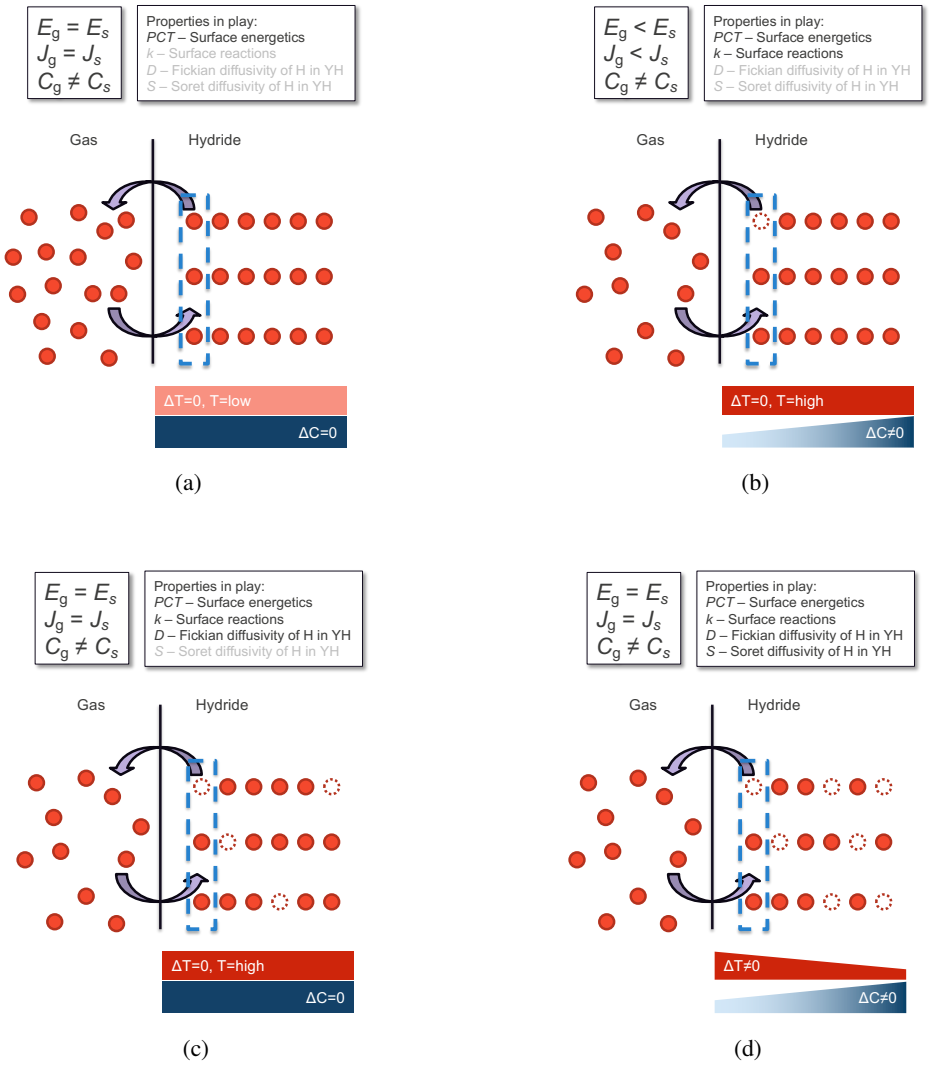

Figure 3.1: Schematics showing process of hydrogen adsorption/desorption and the resulting transport in the bulk material starting with a) equilibrium conditions with gas at low temperature, b) loss of hydrogen in the solid due to elevated temperatures in the gas, c) diffusion of hydrogen through bulk, d) Soret diffusion establishing a concentration gradient in bulk. The active properties are shown for each subfigure, with the properties not contributing to the current state in gray. In addition, the interfacial balancing of energy, E, mass flux, J, and concentration, C, are compared for the gas (g) and the solid (s).

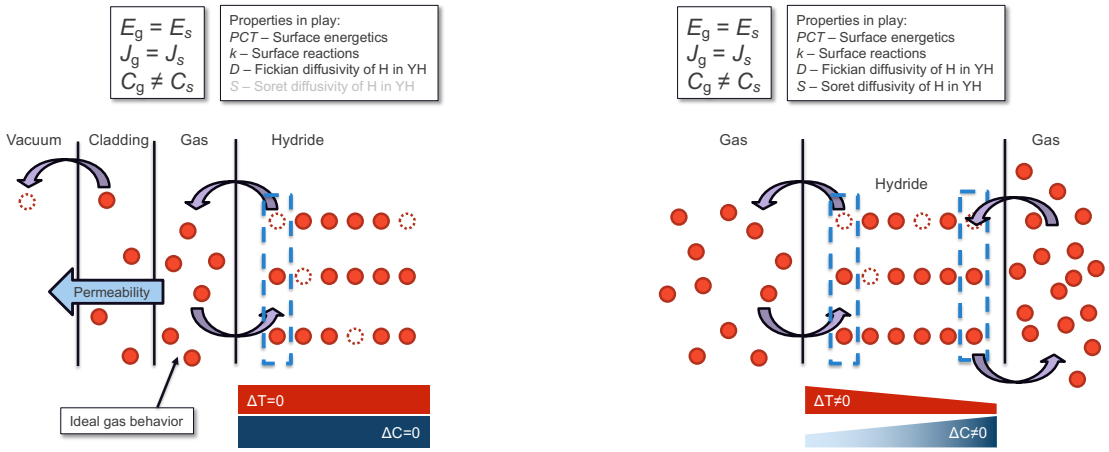

Figure 3.2: Schematics showing the behavior of hydrogen in more complex situations, including a) diffusion into a gap that retains a partial pressure based on the ideal gas law, transport through a cladding based on the permeability of the material, and eventual hydrogen loss into a "vacuum," or environment with effectively zero hydrogen partial pressure; and b) interaction of hydrogen in the presence of a temperature gradient for which the thermodynamics of the system and Soret effect combined result in a concentration gradient. The active properties are shown for each subfigure, with the properties not contributing to the current state in gray. In addition, the interfacial balancing of energy, E, mass flux, J, and concentration, C, are compared for the gas (g) and the solid (s).

cases in Fig. 3.2 that are the most important questions in regards to performance of the material as a moderator. In addition, the non-linearities of the problem – primarily through temperature and concentration dependent properties – motivate the implementation of the physics described here in a nonlinear solver, i.e., `SWIFT`.

3.2 Mathematical Description of Hydride Behavior

The surface interaction of YH_x in a hydrogen environment results in absorption and desorption of hydrogen at the surface of the material. The process may be complex, resulting in reaction rates that are dependent on temperature, surface preparation, non-stoichiometry, partial pressure, etc. In addition, the anharmonicity of hydrogen that occurs with self-interaction may result in complex behavior at the surface and in the bulk [8, 9]. The surface kinetics modeled here will only utilize simple relationships (i.e., Eq. (3.1)) that capture the general behavior of kinetics at the interface – a consequence of only a limited number of experiments exist on the kinetics of YH_x – with the more advanced surface reaction models to be implemented once better data is obtained.

In general, the surface reaction event can be captured via a boundary condition that tracks the surface concentration of hydrogen, C_{surf}, in relation to the equilibrium hydrogen concentration, C_{eq},

$$\frac{\partial C_{surf}(T)}{\partial t} = k[C_{eq}(T) - C_{surf}(T)]. \tag{3.1}$$

The solution for this equation starting from initial surface concentration, C^0, given k is constant, returns,

$$C_{surf}(T) = C_{eq}(T) + (C^0 - C_{eq}(T))\exp(-kt), \tag{3.2}$$

showing that the concentration of hydrogen at the surface will always match the equilibrium hydrogen concentration after enough time has passed, i.e., $C_{surf}(t \to \infty) = C_{eq}(T)$.

Once a concentration gradient is established in the bulk material, Fickian diffusion will act to smooth any gradients in the chemical potential. In addition, the observation of a concentration gradient in the presence of a temperature gradient may indicate that Soret diffusion may also play a role in the bulk material. These two processes can be defined in rate form as,

$$\frac{\partial C_s}{\partial t} = \nabla\left[D(T,x)\nabla C + S(T,x)\nabla T\right], \tag{3.3}$$

where $D(T,x)$ and $S(T,x)$ are the Fickian and Soret diffusion coefficients respectively, which may both be a function of temperature, T, and non-stoichiometry.

For materials that do not form hydrides, such as most steels, permeation through the solid can be used to describe the flux of hydrogen from high to low pressures,

$$\frac{\Phi}{th} = \frac{\text{mol } H_2}{A \cdot time\sqrt{p_{HH}}} = 10^{-9} \text{ for one year, } ZrH_{1.7} \text{ at 1000K} \tag{3.4}$$

where J_∞ is the steady state flux of hydrogen through a barrier, Φ is the permeability of the material, f_{HH} is the fugacity of hydrogen, and t is the thickness of the material. For the temperatures and pressures explored here, the fugacity of hydrogen nearly equals the partial pressure of hydrogen, although mixtures of gases may complicate this assumption [10]. Equation (3.4) is applicable to a barrier exposed to a hydrogen partial pressure, p_{HH}, on one side, and a vacuum on the other, with the square root dependence related to the diatomic behavior of free hydrogen gas.

The gas pressure in the gap can be modeled using the ideal gas law,

$$p_{HH} = \frac{n_h}{2} RT, \tag{3.5}$$

where T is temperature, R is the ideal gas constant, and the molar density of hydrogen, n_h, is divided by two to account for the diatomic nature of hydrogen gas.

For the majority of environments for in-reactor moderator pins, the geometry is small enough that communication of gas throughout the gap between the cladding and the moderator can be assumed to be instantaneous. In other words, there will be no pressure gradient throughout the pin. Consequently, in the presence of a temperature gradient, an inverse gradient in atoms must persist,

$$\frac{\partial C_g}{\partial t} = \nabla \left[\nabla C + \frac{C_g}{T} \nabla T \right] D_g, \tag{3.6}$$

where D_g is a parameter that corresponds to the diffusivity of the gas, but in practice becomes a number, here typically 100, that is large enough to ensure a pressure gradient is not maintained in across the gas gap.

4 Code Implementation

4.1 Model overview

SWIFT utilizes a number of MOOSE capabilities in order to capture the thermochemistry of metal hydrides at high temperature. What follows is an overview of the computational methods used in SWIFT, with a deep dive in to the particular code reserved for code documentation distributed with the code itself.

The fundamental geometry modeled here is a rodlet embedded in a gas plenum, as shown in Fig. 4.1. MOOSE built-in meshing tools are used generate a two dimensional unstructured mesh. Consequently, the results from these simulations typically provide "per meter" information, such as total gas concentration and total permeated gas. While this allows for rapid simulations, it does assume that the interactions at the end caps of the clad moderator can be ignored, and no axial gradients are present, e.g. temperature or pressure gradients. The flexibility of MOOSE allows for extension of the same methods developed here to be applied to 2D-Rz axisymmetric models, which are capable of capturing axial gradients without radial gradients, and 3-D models, which can capture complex gradients throughout entire moderator pin. These different geometries will be explored in future work.

Given the 2-D model utilized here, the majority of the complex thermochemistry occurs at the interfaces. Between the gas gap and the solid metal hydride, the "InterfaceKernel" system in MOOSE is utilized to build a custom model that applies Eq. (3.1) at the boundary. This ensures mass balance by enforcing equal flux out of the gas and into the solid, or vice versa. This model requires a surface reaction rate, and a surface equilibrium condition. These material properties are unique to each metal hydride, and are defined for YH_x in Section 4.2.1.

Concentration gradients in the metal hydride are evolved by built-in MOOSE diffusion kernels, using material specific diffusivities, described in Section 4.2.1. Due to the difficulty in accurately measuring the Soret coefficient, Soret diffusion is ignored in this analysis.

As gas starts to fill the gap, the partial pressure is then computed in each element via the ideal gas law, with pressure gradient smoothed via the use of custom kernels that implement Eq. (3.6).

At the outer most interface – which corresponds here to the boundary between the gas gap and the inner radius of the cladding – a Neumann boundary condition is utilized to account for the permeation of gas through the cladding using Eq. (3.4). Note, the cladding is not incorporated in the models computed here, as the thickness of the material is the only parameter utilized in the boundary condition. In principle, the temperature of the cladding is utilized to compute the permeability, but it can be assumed that the temperature at the inner surface of the cladding can be used to compute the permeability.

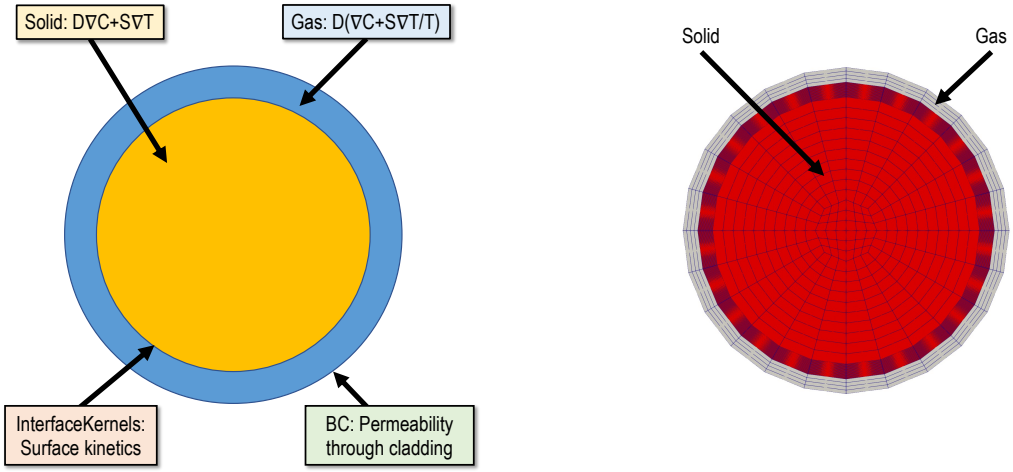

(a) (b)

Figure 4.1: Schematic of the a) idealized geometry and a) 2D mesh utilized in these simulations. Note that the high mesh refinement on the surface of the solid is required to suppress oscillations in the solution.

4.2 Material Properties

4.2.1 Yttrium Hydride

Hydrogen diffusion

Due to its high hydrogen solubility, there have been several experimental studies on the diffusivity of hydrogen in yttrium metal, primarily in context of use as a hydrogen getter. There remains a high-level of scatter in the experimental studies, and details pertaining to the anharmonicity that occurs due to the interaction of hydrogen with itself in solids can possibly result in complex behavior in the presence of high hydrogen concentrations or impurities. In addition, the particular phase of the hydrided yttrium plays a large role in the transport mechanism of hydrogen, thus care must taken in determining from which phase the data was collected.

For YH_x in the range of $1.5 < x < 2$, diffusivities as a function of non-stoichiometry and temperature have been measured via nuclear magnetic resonance [11, 12], and neutron spectroscopy [13]. The activation barrier, Q, and diffusion pre-exponential, D_0, are compiled in Table 4.1, and are used to plot diffusivity as a function of temperature in Fig. 4.2.

In YH_x, it has been identified that diffusivity increases as a function of hydrogen content between $YH_{1.8}$ and YH_2 [6, 13]. This is in contrast to typical vacancy-mediated transport in solids for which diffusivity usually decreases as the number of vacancies are reduced. This dependence has been shown previously [13] at a single low temperature, however the diffusivities compiled in Fig. 4.2 do not indicate a strong correlation between non-stoichiometry and diffusivity.

The data for $YH_{1.63}$ was taken at extremely low temperatures, hence the diffusivity measured by Anderson et al. [12] was likely for a material in the two phase α-Y+γ-YH_x [6].

In the absence of more refined data, the diffusivity of $YH_{2.03}$ will be used as it is the most con-

Table 4.1: Diffusivities of hydrogen in YH_x.

H/Y	Q [eV]	D_0 [m^2/s]	Ref.
1.63	1.1	$5.3 \cdot 10^{-5}$	[12]
1.91	0.53	$4.8 \cdot 10^{-8}$	[11]
1.92	0.438	$7.9 \cdot 10^{-9}$	[12]
1.95	0.4	$9.0 \cdot 10^{-9}$	[11]
1.97	0.29	$1.46 \cdot 10^{-8}$	[13]
1.98	0.417	$7.9 \cdot 10^{-9}$	[12]
2.03	0.38	$1.0 \cdot 10^{-8}$	[11]

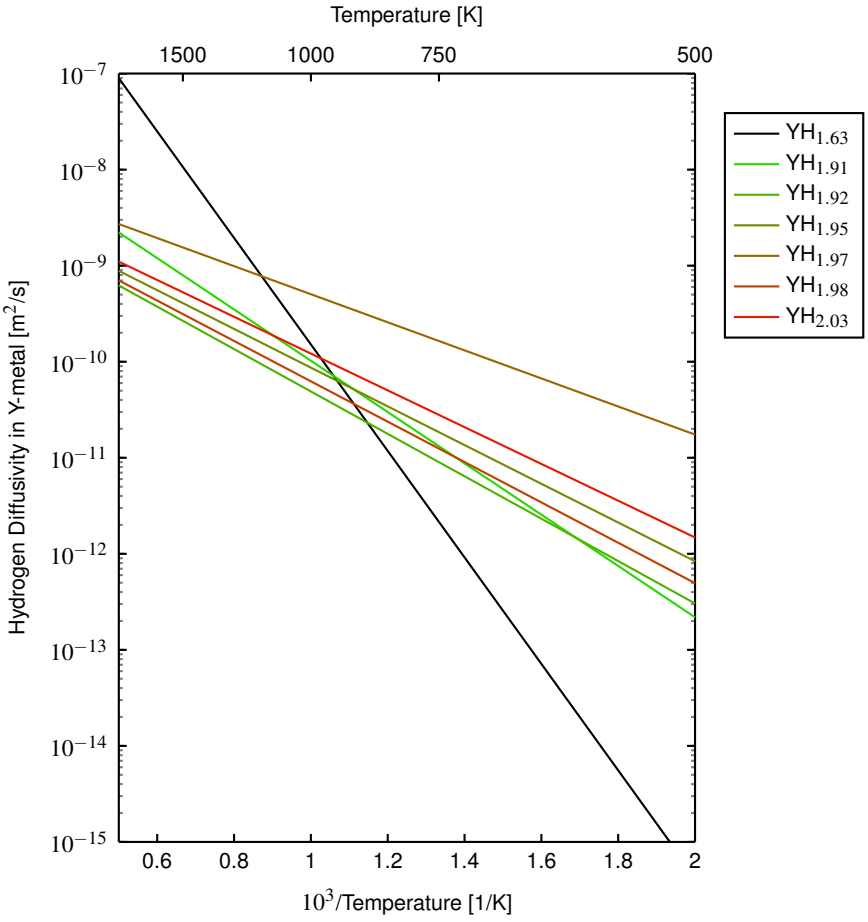

Figure 4.2: Diffusivity of hydrogen in YH_x using the diffusivities in Table 4.1.

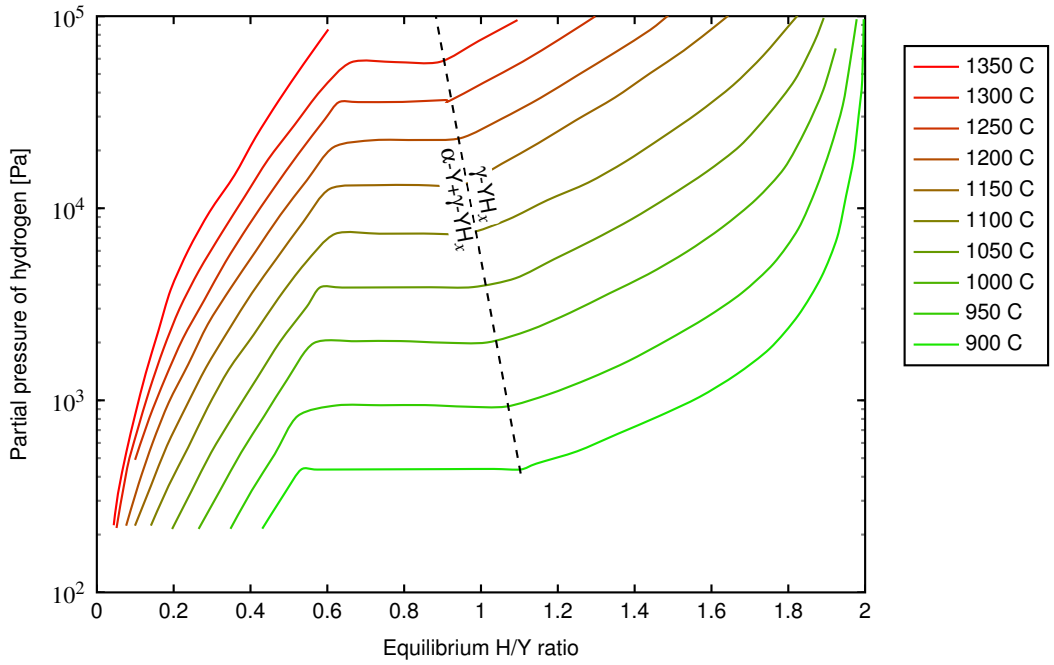

Figure 4.3: PCT curves from Lundin and Blackledge [14]. The black dashed line shows the separation between the two phase α-Y+γ-YH$_x$ and γ-YH$_x$ regions.

servative value in the band of similar diffusivities over the temperatures of interest (< 1000 K).

PCT curves

Pressure-composition-temperature curves, or so called PCT curves are an extremely useful tool in determining the relationship between the non-stoichiometry of YH$_x$ and its environment. The data is typically plotted as a series of isothermal curves as a function of non-stoichiometry, as shown in Fig. 4.3.

In the case of the non-linear behavior in `SWIFT`, it is more desirable to be able to compute the equilibrium concentration as a function of temperature and partial pressure. Typically, YH$_x$ is kept in the single phase region close to YH$_2$ in order to maintain mechanical stability. This allows the data from Lundin and Blackledge [14] to be isolated to the single γ-YH$_x$ phase region, removing much of the complexity of the PCT curves, including the so called "plateau" – in which a wide range of compositions can be produced via small changes in partial pressure – and the yttrium metal region below $\sim$YH$_{0.5}$. The hydrogen partial pressure as a function of temperature for which the single-phase YH$_x$ structure begins can be extracted from the PCT data by taking the point at which the plateau region ends, roughly outlined in Fig. 4.3. The extracted data exhibits the behavior of a second order polynomial,

$$p^0_{HH}\ [\text{Pa}] = \exp(-26.1 + 3.88 \cdot 10^{-2} T - 9.7 \cdot 10^{-6} T^2), \tag{4.1}$$

where T is temperature in [K], as plotted in Fig. 4.4.

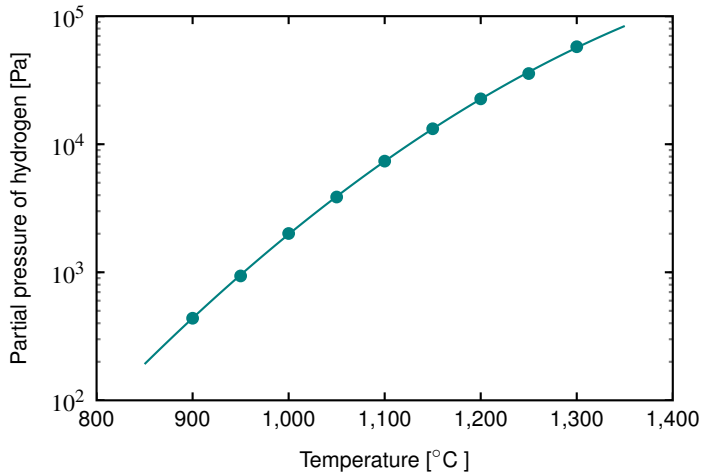

Figure 4.4: Partial pressure of hydrogen in YH_x as a function of temperature that signifies the transition to the single-phase region, as extracted from the PCT curves from Lundin and Blackledge [14].

An analytical expression for the single phase γ-YH_x region has been fit to the Lundin and Blackledge data as a function of temperature and partial pressure of hydrogen:

$$C_{eq}\,[\mathrm{H/Y}] = 2 - \left(1 + \exp\left[21.6 - 0.0225T + \left(-0.0445 + 7.18\cdot 10^{-4}T\right) g(p_{HH})\right]\right)^{-1}, \quad (4.2)$$

where T is in [K] and p_{HH} is in [Pa], and $g(p_{HH}) = \ln\left(p_{HH} - p^0_{HH}\right)$. Eq. (4.2) is only valid between $1 \leq C_{eq} \leq 2$ and $T \leq 1573$K, At temperatures below 1173K, Eq. (4.2) can be extrapolated with some confidence, but additional data is needed to ensure the applicability of the fit.

Surface kinetics

Surface kinetic parameters that can be used to calculate adsorption and desorption of hydrogen from YH_x are not readily available. In the absence of such values, reactions with hydrogen and yttrium metal up to a H/Y ratio of 0.35 can be used, although the different phase and transport mechanism (interstitial rather than vacancy mediated diffusion) likely means the reaction rates can only be used here as a estimated stand-in value. Further work must be completed in the expected non-stoichiometry ranges of YH_x in order to fully capture the nonlinear behavior of adsorption and desorption. Fortunately, the surface reaction in metal hydrides, and YH_x in particular, is extremely rapid. Consequently, the transient behavior of YH_x will be diffusion-limited, and the relative importance of accurate surface reaction rates is much smaller than the need for accurate diffusivities.

Fisher and Tanase performed a series of reaction experiments in which a sample of yttrium metal was subjected to a hydrogen partial pressure equal to approximately 0.35 H/Y at various temperatures in order to determine the surface kinetics and diffusion of hydrogen in Y [8]. While these experiments were performed on samples of yttrium starting with a stoichiometry of 0, and only going to $YH_{0.35}$, these experiments can provide an initial guess at the surface absorption of hydrogen.

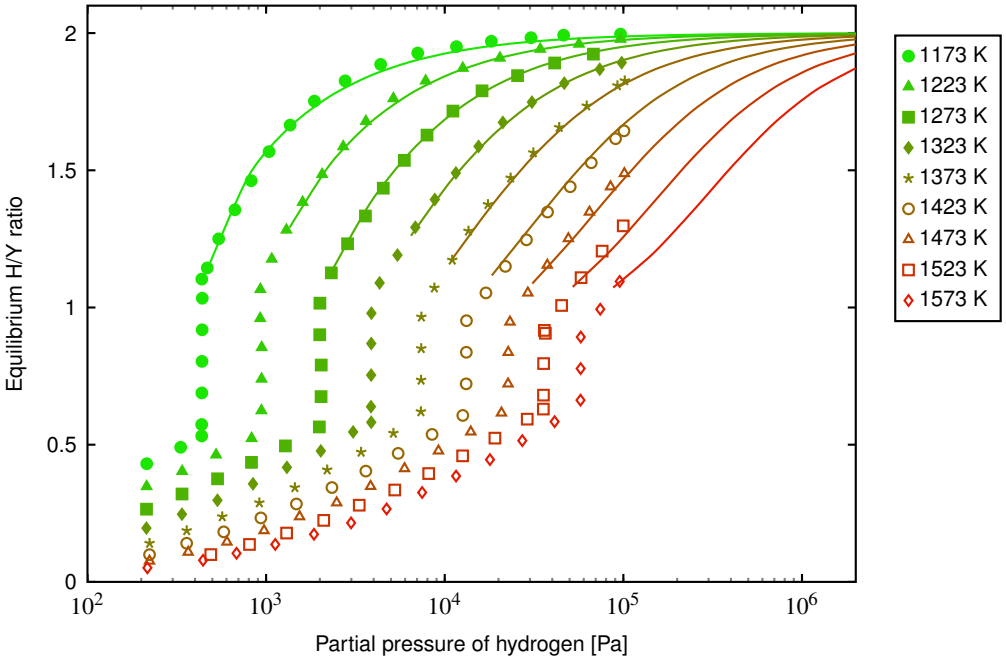

Figure 4.5: PCT curves data from Lundin and Blackledge [14] as a function of temperature and hydrogen partial pressure provided as points, with the analytical fit from Eq. (4.2) as lines.

The surface reaction rate was determined by comparing the analytical expression for hydriding of yttrium metal by Fisher and Tanase [8], similar to Eq. (3.2) where $C^0 = 0$. This led to k values as displaced in Fig. 4.6, with an analytical expression given by,

$$k[1/\mathrm{s}] = 4.95 \cdot 10^5 \exp\left(-1.52/k_B T\right). \tag{4.3}$$

Although there is a relatively high degree of scatter in k, excellent reproduction with the experimental curves of hydrogen non-stoichiometry in yttrium as a function of time by Fisher and Tanase indicates that the surface reaction (and corresponding diffusivity) is likely independent of hydrogen concentration at the low relative hydrogen concentrations analyzed by Fisher and Tanase [8]/

4.2.2 Cladding permeabilities

The permeability of hydrogen through membranes, claddings, and barriers has been studied extensively. A subset of this information is reproduced here in Table 4.2 and Fig. 4.7 as a scoping tool for comparison between materials. Further refinement of the permeabilities is necessary for any real design application as the details of applicability, material specifications, and experimental techniques may need further refinement.

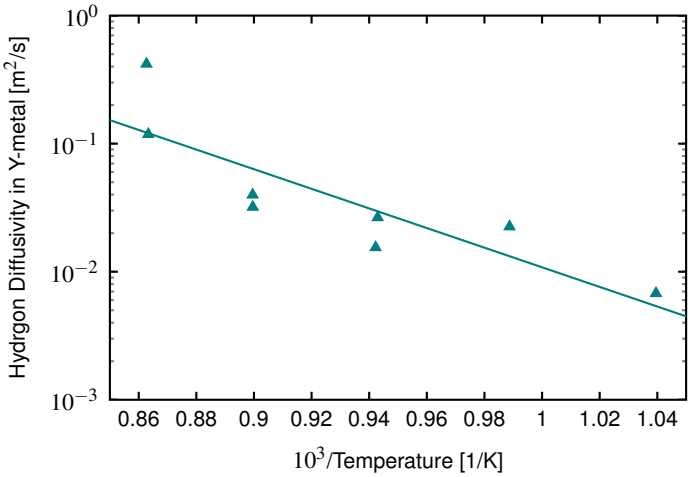

Figure 4.6: Surface absorption reaction coefficient in yttrium metal [8].

Table 4.2: Permeabilities of hydrogen through a variety of materials.

Material	$D_0 \left[\frac{\text{mol } H_2}{\text{m·s}\sqrt{\text{Pa}}}\right]$	Q [kJ/mol]	Temperature range [$^\circ C$]	Ref.
Aus. SS	$1.2{\cdot}10^{-4}$	59.8	150-427	[15]
Ag	$2.21{\cdot}10^{-7}$	86.8	100 -	[16]
Al	$5.80 \cdot 10^{-5}$	123	420 - 520	[16]
Al_2O_3	$3.3{\cdot}10^{-10}$	97.4	1000 - 1400	[17]
Au	$3.10 \cdot 10^{-6}$	123		[16]
Be	$1 \cdot 10^{-6}$	73		[18]
Co	$6.30 \cdot 10^{-9}$	57.0	470 - 670	[16]
Co	$3.80 \cdot 10^{-8}$	64.4	470 - 820	[16]
Cu	$5.86{\cdot}10^{-7}$	75.7	470 - 970	[16]
Fe	$4.10 \cdot 10^{-8}$	34.9	330 - 770	[16]
Mo	$2.30 \cdot 10^{-7}$	80.7	500 - 1700	[16]
Ni	$3.22{\cdot}10^{-7}$	54.8	300 - 775	[16]
Nb	$6.30 \cdot 10^{-9}$	-35.5	400 - 600	[16]
Pd	$2.20 \cdot 10^{-7}$	15.7	300 - 709	[16]
Pt	$1.20{\cdot}10^{-7}$	70.7	540 - 900	[16]
Si	$1.40 \cdot 10^{-5}$	225	1240 - 1485	[16]
Ta	$5.80 \cdot 10^{-9}$	-20.2	350 -	[16]
W	$7.80 \cdot 10^{-7}$	141	1100 - 2900	[16]
V	$4.00 \cdot 10^{-9}$	-24.9	300 -	[16]

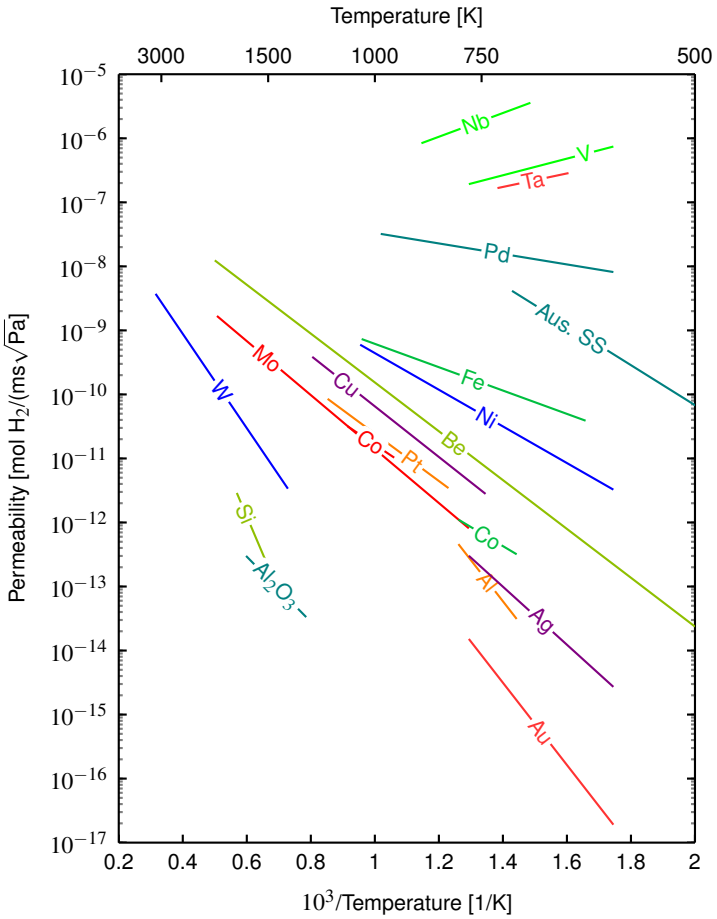

Figure 4.7: Permeability of hydrogen in through various materials [15–18]. Note that there are many details on the applicability and accuracy of this data contained in [16] and the associated references therein.

5 Results

5.1 Hydrogen Loss Through Cladding

In order to fully exercise the capabilities recently added into SWIFT, the hydrogen evolution of YH_x in a cladding tube was simulated to capture the gap/solid reactions and eventual permeation through the cladding. This baseline simulation utilized a one centimeter radius rod of $YH_{1.8}$ in an evacuated Mo tube. A one millimeter gap between the solid hydride and cladding is maintained with a one millimeter thick Mo wall. As discussed in Section 4.1, a 2D mesh was utilized in which gas content is tracked. By ignoring the top and bottom interactions of the pin, these rapid 2D simulations can provide similar concentrations as would a 3D simulation, while providing a "per-meter" basis for mole content, e.g. moles lost through the cladding. An average temperature of 1300°C was utilized, with a temperature gradient of 50°C across the entire mesh in the x-direction, as shown in Fig. 5.1.

In order to evaluate the impact of the permeation through the cladding, two simulations were run in which permeability through the one millimeter Mo tube occurred, and one where no hydrogen loss from the system boundary was allowed. For the two cases (with and without permeability), the average and surface equilibrium non-stoichiometry over time are co-plotted in Fig. 5.2, with the hydrogen partial pressure over time plotted in Fig. 5.3. In addition, the hydrogen concentration in the solid, gas, and lost via permeation as a function of time is shown in Fig. 5.4. Finally, the 2D evolution of the non-stoichiometry is shown in Fig. 5.5.

As soon as the simulation begins, the metal hydride starts to lose hydrogen due to an extremely small C_{eq}, as mandated by the low partial pressure (i.e., initially vacuum). As dehydriding continues, the partial pressure slowly increases, increasing C_{eq} to eventually approach the average non-stoichiometry at around a half a minute (Fig. 5.3). A slight gradient in the relative hydrogen concentration is evident early in the simulation as well (Figs. 5.5a and 5.5b) due to the temperature dependence of the PCT curves resulting in a gradient in C_{eq}. Note that hydrogen partial pressure remains spatially flat across the simulation due following Eq. (3.6). At this point, if permeation were not possible through the cladding, the hydrogen partial pressure and corresponding non-stoichiometries would reach a steady state after about an hour, as indicated by the dashed lines in Figs. 5.2 and 5.3. However, due to the steady loss of hydrogen out of the cladding, a decrease in partial pressure and total system hydrogen content starts to dominate the non-stoichiometry of the YH_x, leading to an eventual decrease to $YH_{1.5}$ around 50 hours. The transition from vacuum, equilibrium with the solid, and eventual loss is clearly shown in the gas content line in Fig. 5.4.

Throughout the simulation, the simulations show a concentration gradient in the YH_x. Note that although Soret diffusion is an effect that has been measured before, it has not been included here. The concentration gradient shown in Fig. 5.5 is due entirely to the thermochemistry of the system driving the equilibrium surface concentration. In the case of the non-permeating

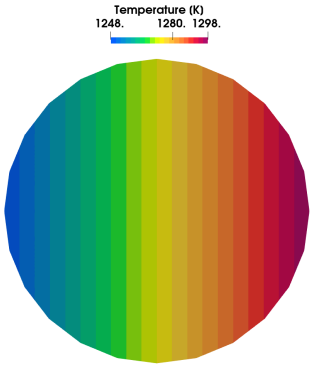

Figure 5.1: Temperature gradient for the 2D rodlet geometry. Note, a smooth temperature transition is maintained across the solid YH_x interface, an approximation that will need to be refined in later work.

cladding, the final equilibrium concentration gradient is $YH_{1.85}$ to $YH_{1.74}$, over a 46°C temperature gradient. In this case, the temperature dependence of the PCT curves essentially transports the hydrogen from the right to the left side of the pellet, with only minimal amounts of hydrogen remaining in the gap to maintain the equilibrium hydrogen partial pressure. In the simulation where permeability is allowed, similar non-stoichiometry gradients persist.

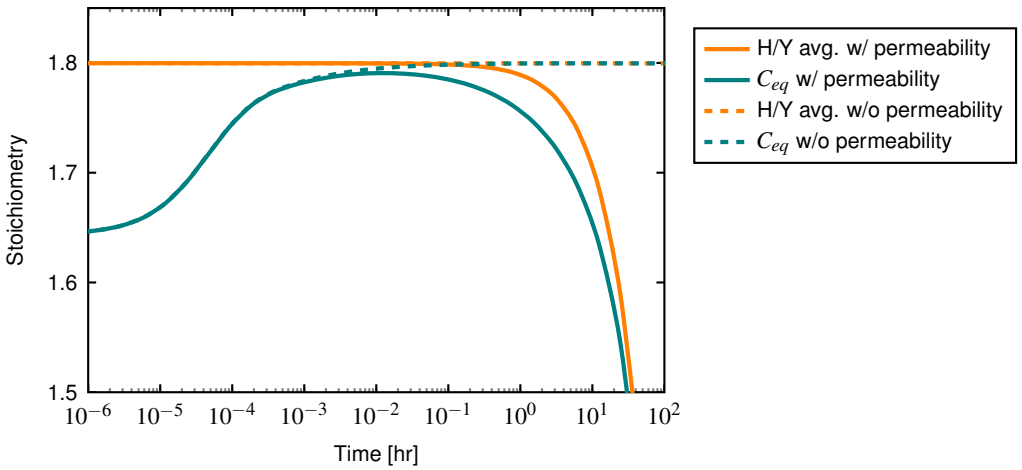

Figure 5.2: Non-stoichiometry and surface equilibrium conditions for the simulations with (solid) and without (dashed) permeable claddings.

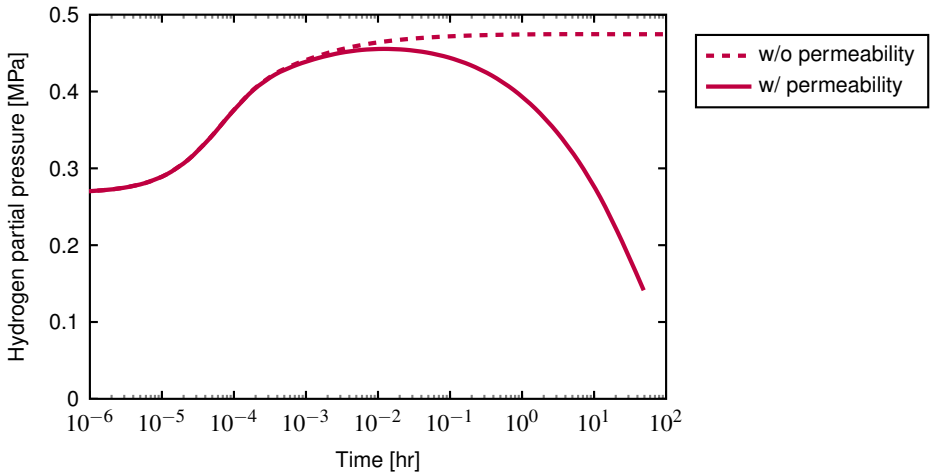

Figure 5.3: Hydrogen partial pressures for the simulations with (solid) and without (dashed) permeable claddings.

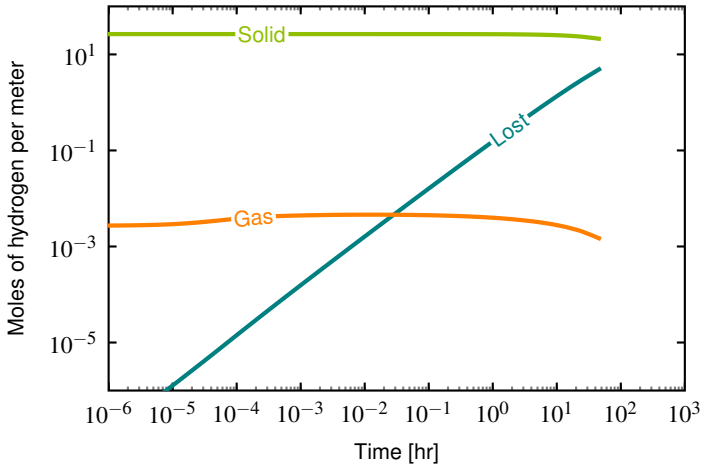

Figure 5.4: Hydrogen gas content as a function of time for the simulation with the permeable cladding. Here, the hydrogen that permeates through the cladding is assumed to be "lost" to the system.

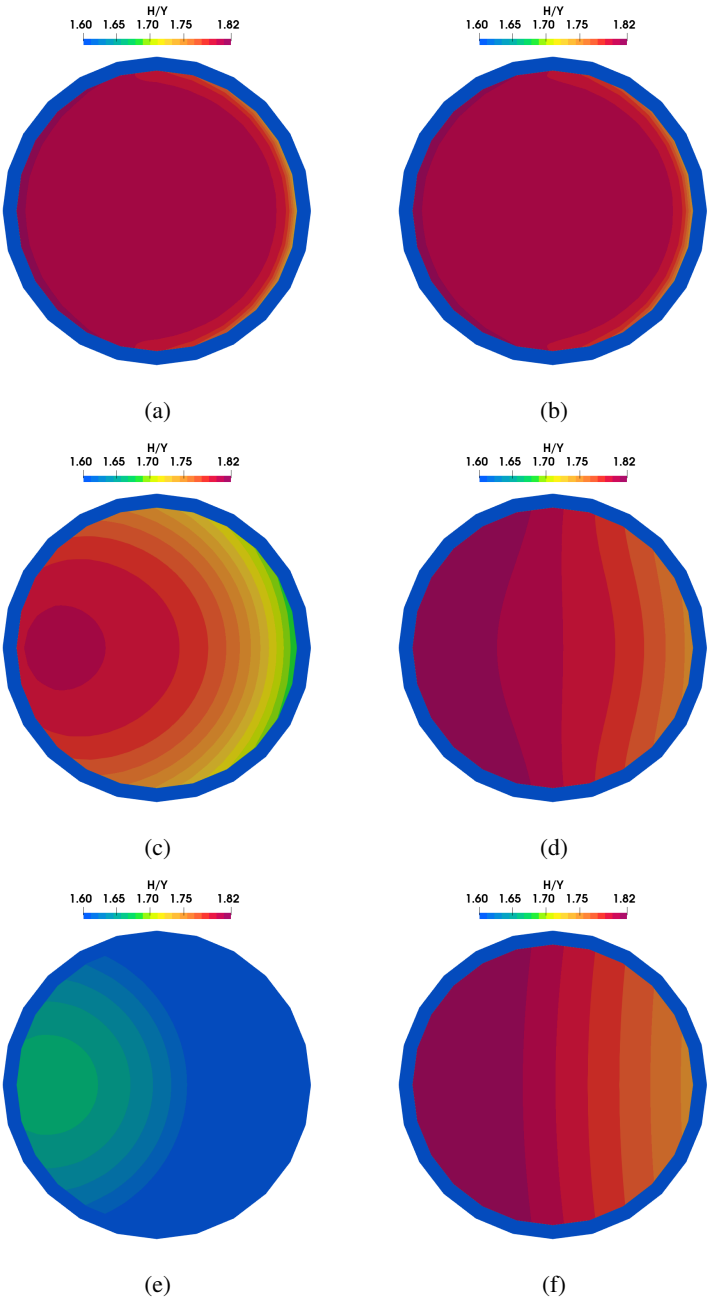

Figure 5.5: Evolution of the non-stoichiometry of YH_x at a,b) simulation start, b) 9 minutes, c,d) 9 hours, and e,f) 75 hours. The left and right columns correspond to the simulations with and without permeable claddings, respectively.

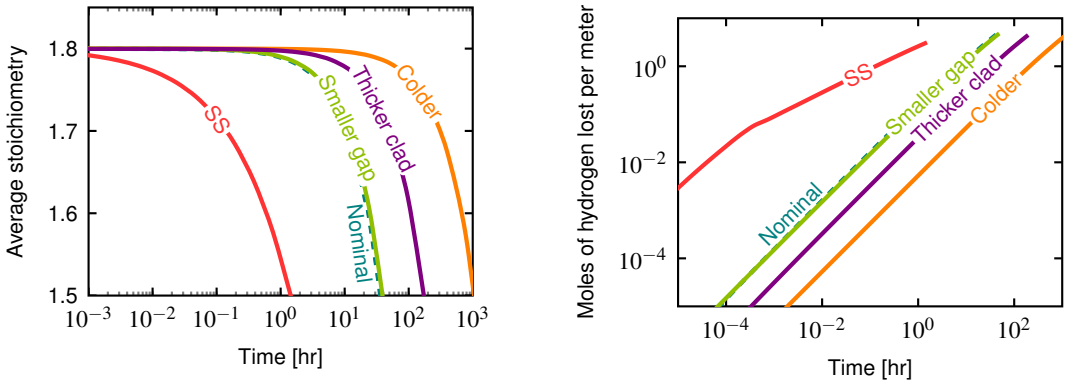

(a) (b)

Figure 5.6: The impacts for several hydrogen loss mitigation techniques over time; a) average stoichiometry and b) total hydrogen lost per meter of moderator.

5.2 Hydrogen Loss Mitigation

One of the primary physical attributes that makes metal hydrides difficult for use as reactor moderators is the eventual permeation of hydrogen through many of the hydride pin cladding candidates. Through the simulations in Section 5.1, a one millimeter thick Mo tube results in an unmanageable loss of hydrogen within a day. In order to increase the service time of the YH_x, several design parameters can be tweaked including reducing the gap size to 0.5 millimeters, using a thicker 5 millemeter cladding, or reducing the temperature of the moderator from 1300°C to 1000°C. The impacts of these types of mitigation techniques are shown in Figs. 5.6a and 5.6b, along with the consequence of utilizing a much more permeable cladding material like stainless steel.

5.3 Empire example core

`SWIFT` was built using the `MOOSE` framework for the explicit purpose of multi-physics coupling. As a first introduction into the applicability of `SWIFT` – specifically the ability to estimate hydrogen content in a metal hydride during nuclear reactor operation – the stoichiometry of YH_x was tracked for the prototypical microreactor "empire" core design [19]. A rodlet of initially $YH_{1.95}$ with a radius of 8.25 mm and length of 1.6 m was subjected to an example temperature gradient, as plotted in Fig. 5.7. The gas volume was defined by a 0.5 mm gap between the moderator and the casing, as well as a centimeter-sized gap from the top and bottom of the moderator from the casing. The cylindrical geometry of the problem was utilized by simulating a 2D-Rz axisymmetric simulation, which requires considerably fewer mesh elements than a full 3D simulation. A second simulation for which permeability is allowed through through a 0.25 mm thick SS-316 cladding is provided for comparison.

Starting from a hydrogen partial pressure of zero, the rod evolves to maintain a stoichiometry that varies from 1.93 to 1.98, as shown in Fig. 5.7. This steady-state stoichiometry essentially

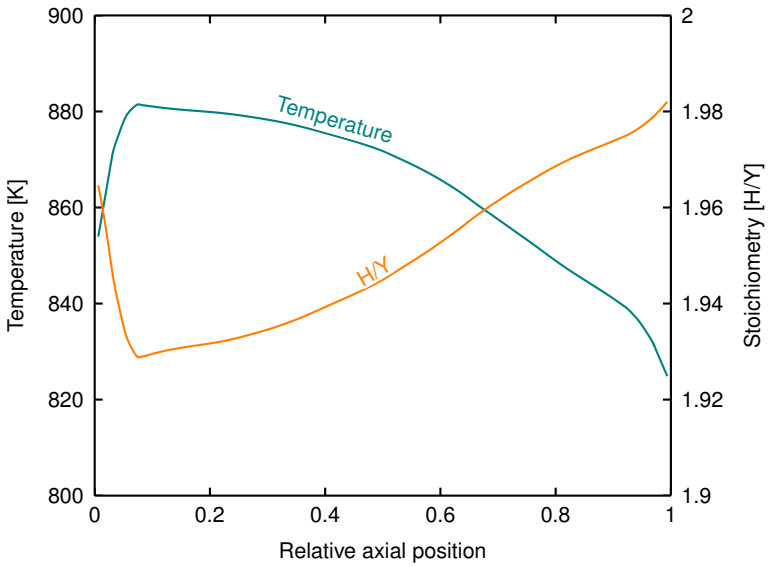

Figure 5.7: Example temperature profile for a "empire" yttrium hydride moderator rodlet and steady-state stoichiometry as a function of axial position if permeability is ignored.

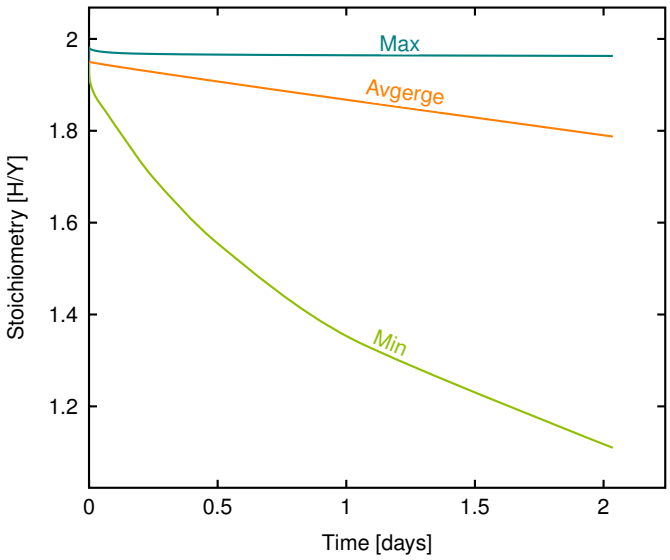

Figure 5.8: Maximum, minimum, and average rodlet as a function of time is permeability is allowed through the stainless steel casing.

follows the inverse of the temperature profile and is determined by the 5 Pa isobaric PCT curve, which is set by the equilibrium plenum hydrogen partial pressure. The steady-state hydrogen concentration results after about a week of time at the set temperature. This pressure is nearly constant throughout the rodlet plenum via the pressure equalizing equation in Eq. (3.6).

If permeability through the stainless steel casing is allowed, the stoichiometry drops rapidly, resulting in an outside surface stoichiometry minimum that reaches 1.0 in about two days, as shown in Fig. 5.8. Clearly, other hydrogen barriers will be required to ensure that the metal hydrides retain enough hydrogen to be effective moderators.

6 Discussion and Conclusions

While each individual piece of physics that drives the kinetics of hydrogen in metal hydrides is not in itself complex, the interconnection of the system with the gas gap and cladding results in coupled nonlinear behavior that can be nontrivial to compute. These pieces of physics, along with best estimates of material properties that are needed as input into the various mathematical descriptions of the phenomena, have been compiled here and implemented into SWIFT. Using only a handful of simulations, the usefulness of such a code was shown to produce plots useful for reactor designers and simulations that showed the nonlinear behavior of the non-stoichiometry within the solid YH_x.

It is clear that the simulations presented here are only as good as the material properties that are supplied. Due to the nature of the PCT curves themselves, it is difficult to get accurate properties as a function of non-stoichiometry, even though there are indications that transport of hydrogen does depend on the ratio of hydrogen to metal. Due to this difficulty, a tool such as SWIFT may be essential to detangle the different phenomena. This is likely most prominent in the determination of the impact of the temperature gradient on the transport of hydrogen.

One of the primary outcomes of this work was to show that the concentration gradient observed in metal hydrides subject to a temperature gradient cannot be attributed to a Soret type of diffusion alone; the thermochemistry of the system necessitates a complex equilibrium state across the entire material, not just at a single surface. Consequently, measurement of Soret coefficient due purely to measurement of the concentration gradient under temperature will result in a property that can accurately capture the concentration gradient as a function of the temperature gradient in only one configuration and environment, namely that of the experiment itself. As the need grows for advanced modeling and simulation to share more of the burden associated with reactor design and safety analysis, the desire for mechanistic models will continue to expand. As such, the identification of all prominent phenomen at play must be separately addressed in a realistic and meaningful manner.

Acknowledgements

This work was sponsored by the U.S. Department of Energy, Office of Nuclear Energy, Nuclear Energy Advanced Modeling and Simulation (NEAMS) program. Los Alamos National Laboratory, an affirmative action/equal opportunity employer, is operated by Triad National Security, LLC, for the National Nuclear Security Administration of the U.S. Department of Energy under Contract No. 89233218CNA000001.

References

[1] W. M. MUELLER, Chapter 2 - hydrides in nuclear reactor applications, in: W. M. Mueller, J. P. Blackledge, G. G. Libowitz (Eds.), Metal Hydrides, Academic Press, 1968, pp. 21–50. doi:https://doi.org/10.1016/B978-1-4832-3215-7.50006-X.
URL https://www.sciencedirect.com/science/article/pii/B978148323215750006X

[2] C. J. Permann, D. R. Gaston, D. Andrs, R. W. Carlsen, F. Kong, A. D. Lindsay, J. M. Miller, J. W. Peterson, A. E. Slaughter, R. H. Stogner, R. C. Martineau, MOOSE: Enabling massively parallel multiphysics simulation, SoftwareX 11 (2020) 100430.

[3] J. P. BLACKLEDGE, Chapter 10 - yttrium and scandium hydrides, in: W. M. Mueller, J. P. Blackledge, G. G. Libowitz (Eds.), Metal Hydrides, Academic Press, 1968, pp. 441–489. doi:https://doi.org/10.1016/B978-1-4832-3215-7.50014-9.
URL https://www.sciencedirect.com/science/article/pii/B9781483232157500149

[4] R. A. Johnson, W. T. Morgan, S. R. Rocklin, Design, ground test and flight test of snap 10a, first reactor in space, Nuclear Engineering and Design 5 (1) (1967) 7–21. doi:https://doi.org/10.1016/0029-5493(67)90074-X.
URL https://www.sciencedirect.com/science/article/pii/002954936790074X

[5] D. Olander, E. Greenspan, H. D. Garkisch, B. Petrovic, Uranium–zirconium hydride fuel properties, Nuclear Engineering and Design 239 (8) (2009) 1406–1424, hydride Fueled LWRs. doi:https://doi.org/10.1016/j.nucengdes.2009.04.001.
URL https://www.sciencedirect.com/science/article/pii/S0029549309001745

[6] A. P. Shivprasad, T. E. Cutler, J. K. Jewell, V. K. Mehta, S. W. Paisner, C. A. Taylor, C. N. Taylor, H. R. Trellue, D. W. Wootan, E. P. Luther, Advanced Moderator Material Handbook, Tech. Rep. LA-UR- 20-27683 (Sep. 2020).

[7] S. S. Mohammadshahi, E. M. Gray, C. J. Webb, A review of mathematical modelling of metal-hydride systems for hydrogen storage applications, International Journal of Hydrogen Energy 41 (5) (2016) 3470–3484.

[8] P. W. Fisher, M. Tanase, Diffusivities of Hydrogen in Yttrium and Yttrium Alloys, Journal of Nuclear Materials 122-123 (1984) 1536–1540.

[9] T. Maeda, S. Naito, M. Yamamoto, M. Mabuchi, T. Hashino, Diffusivity and solubility of hydrogen and deuterium in yttrium, Journal of the Chemical Society, Faraday Transactions 89 (24) (1993) 4375–4379.

[10] C. S. Marchi, B. P. Somerday, Thermodynamics of Gaseous Hydrogen and Hydrogen Transport in Metals, MRS Proceedings 1098 (1) (2008) 1–12.

[11] G. Majer, J. Gottwald, D. T. Peterson, R. G. Barnes, Model-independent measurements of hydrogen diffusivity in the yttrium dihydrides, Journal of Alloys and Compounds 330-332 (2002) 438–442.

[12] D. L. Anderson, R. G. Barnes, T. Y. Hwang, D. T. Peterson, D. R. Torgeson, Hydrogen Locations, Diffusion and the Electronic Density of States in Yttrium Dihydrdies: A Nuclear Magnetic Resonance Investigation, Journal of Less-Common Metals 73 (1980) 243–251.

[13] U. Stuhr, D. Steinbinder, H. Wipf, B. Frick, Hydrogen Diffusion in f.c.c. TiH xand YH x: Two Distinct Examples for Diffusion in a Concentrated Lattice Gas, Europhysics Letters (EPL) 20 (2) (1992) 117–123.

[14] C. E. Lundin, J. P. Blackledge, Pressure-Temperature-Composition Relationships of the Yttrium-Hydrogen System, Journal of The Electrochemical Society 109 (9) (1962) 838–5.

[15] C. S. Marchi, B. P. Somerday, Technical Reference for Hydrogen Compatibility of Materials, Tech. Rep. SAND2012-7321 (Sep. 2012).

[16] S. A. Steward, Review of Hydrogen Isotope Permeability Through Materials (1983) 1–28.

[17] A. C. Bini, G. Cosoli, L. Pilloni, Hydrogen Permeation Measurements on Alumina (2004) 1–4.

[18] K. Kizu, K. Miyazaki, T. Tanabe, Hydrogen Permeation and Diffusion in Beryllium, Fusion Technology 28 (1995) 1205–1210.

[19] C. Matthews, V. Laboure, M. DeHart, J. Hansel, D. Andrs, Y. Wang, J. Ortensi, R. C. Martineau, Coupled Multiphysics Simulations of Heat Pipe Microreactors Using DireWolf, Nuclear Technology 207 (7) (2021) 1142–1162.